Available online at www.CivileJournal.org

Civil Engineering Journal

(E-ISSN: 2476-3055; ISSN: 2676-6957)

Vol. 10, No. 01, January, 2024

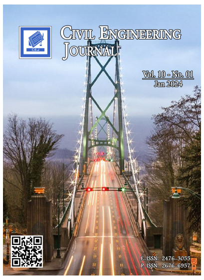

Experimental and Numerical Study of Soil Strata for Underground Transportation System: A Case Study

Osamah Alqawas [1, 2], Md. Rehan Sadique [2], Zaid Mohammad [2*], Sanan Husain Khan [3*]

[1] *Department of Engineering Management and Entrepreneurships, College of Engineering, Debrecen University, Debrecen, 4028, Hungary.*

[2] *Department of Civil Engineering, Z.H. College of Engineering and Technology, Aligarh Muslim University, Aligarh, 202002, India.*

[3] *Department of Mechanical and Aerospace Engineering, United Arab Emirates University, Al-Ain, Abu Dhabi, 15551, UAE.*

Received 30 September 2023; Revised 13 December 2023; Accepted 22 December 2023; Published 01 January 2024

Abstract

In the current capital of Yemen, Sana'a, a time-efficient and economical transportation system is one of the greatest challenges to overcome the increasing urbanization for many years. Rapid transport systems use tunnel structures to reach the city's most inaccessible areas. Given the Gulf's geopolitical unrest, these structures could also serve as emergency shelters. Consequently, this research conducted an experimental soil exploration investigation in Sana'a, Yemen, to identify potential tunneling sites for the city's rapid transit system. The field exploration, in-situ, and laboratory soil testing at the four locations were performed with the collaboration of the Ministry of Public Works & Highways, Yemen. Further, to calculate the geotechnical parameters for tunnel design, numerical analysis has been carried out using the finite element package ABAQUS, and two-dimensional plane-strain numerical models of underground tunnel structure have been developed to conduct the parametric study in different soil types and boundary conditions under static loading. The material behavior of soil strata has been incorporated into the well-known Mohr-Coulomb constitutive model. The field investigation found that the geotechnical properties of the soil strata in Sana'a have a lot of variation. The numerical study shows that the maximum deformation in the concrete liner of the tunnel was observed at the crown of the tunnel. The ovalling effect in tunnel concrete liner was also seen in all the tunnel models, and the maximum ground settlement at sites 1, 2, 3, and 4 was estimated to be approximately 4, 25, 17, and 11 mm, respectively.

Keywords: ABAQUS; Deformation; Tunnel; Field Exploration; Static Loading; Finite Element Model.

1. Introduction

As the population continues to grow, there will be a greater demand for additional housing as well as associated infrastructural amenities. This will require an increasing amount of surface area. In order to combat urban sprawl in metropolitan areas, traffic congestion and the development of public transportation have progressed over time. Underground space creation, in particular the construction of tunnels, has become a cost-effective and alternative solution to overground challenges. This is especially true when dealing with issues such as traffic congestion, the acquisition of land, and the disturbance of urban activities. The construction of subterranean tunnels in rock and soil has been accelerated as a result of recent technological advancements in excavation. These days, common excavation techniques for soil include "Cut and Cover," "Box Jacketing," and "Pressure Balancing Machine," while common excavation techniques for rocks include "Drilling and Blasting", "Sequential Excavation Technique" and "Mechanized

* Corresponding author: zmohammad_co@myamu.ac.in; shkhan@uaeu.ac.ae

http://dx.doi.org/10.28991/CEJ-2024-010-01-03

Tunneling" using a tunnel boring machine (TBM) [1]. Nunes and Meguid [2] conducted an investigation into the effects that topping sandy layers might have on a tunnel that was dug through softer ground. They were able to conclude that, when compared to the scenario with homogeneous clay, the bending stresses were reduced by nearly 70% when the stiff layer (sand) was found close to the tunnel.

According to the findings of Mazek & Almannaei [3], they have shown that the volume loss in stratified soil had an effect on the deformation and stresses of the underground opening. This was measured as the ratio of the difference between the volume of excavated soil and the volume of the tunnel over the volume of excavated soil. They found out that a loss of volume ranging from 1.5 to 4.5% had an effect on the stress and displacement in underground openings. Since analytical solutions are sometimes unavailable, conformal mapping techniques are crucial for stress and displacement analysis of tunnels of any shape. The study introduces numerical conformal mapping methods, including Symm's. Numerical examples of U-shaped and rectangle tunnels show the method's accuracy and adaptability to real circumstances [4]. Zhang et al. [5] had also examined the effect of the multi-layered soils on the lining behavior, specifically looking at how the relative stiffness of the strata and the thickness of the layers affected the lining. It had been observed that, for two-layered soil conditions, an increase in the relative stiffness of the overlying sandy layer leads to approximately a 45% reduction of the bending moment and a 50% reduction of the convergence. On the other hand, for three-layered soil conditions, an increase in the relative thickness of the sandwiched clay layer causes a rise of approximately 90% of both the moment and the convergence. Both results were found to be consistent with the hypothesis. Zhao et al. [6] examined spalling, a stress-induced brittle fracture at tunnel entrances in hard rock masses. The study examines spalling strength, failure depth, excavation-damaged zones (EDZ), and cross-section morphologies in 29 gneissic granite examples. The results show that EDZ greatly influences tangential stress, causing deeper failures. EDZ increases spalling failure depth by 1.85 to 2.18 times in D- and Horse-shoe tunnels. Comparisons with in-situ geophysical testing reveal present approaches may overestimate. The study reveals that D-shape tunnels prevent spalling better than Horseshoe tunnels in hard and brittle rock masses. The interaction between the soil and the structure of the soil was a significant factor in the improvement of the estimated surface settlement trough for Shanghai soft clay in layered soil. Accurate predictions of the sectional forces, moment, and deformation of the tunnel support system are necessary for the system to work optimally [7].

Esmaeili et al. [8] examine optimal fiberglass dowel arrangements for tunnel face stability in layered soil. Horizontal layering has higher extrusion than vertical layering and rises with lower soil elasticity modulus. Initial stress variations considerably affect tunnel face extrusion, but fiberglass dowel angle adjustments have little effect. The study stresses the importance of soil conditions and initial stress in tunnel face stability optimization. In order to facilitate a sensible and economically efficient design of the support system for a soft ground tunnel, several studies have been conducted to investigate the impact of various parameters in static analysis [9–13]. The result for determining the horizontal and vertical displacement was modified due to the interaction between the soil and the structure. When compared to the green field condition that was analyzed by Bian et al. [14], the horizontal displacement had increased by 21% in the layered soil. This was due to the fact that the soil-structure interaction was taken into consideration. Numerous authors Azadiab [15], Abdel-Motaal et al. [16], Gomes et al. [17], have investigated the effect that seismic waves have on liners in stratified soil. The relative position of the stiff layer in relation to the vicinity of the aperture has a major impact on the stability of the tunnel liner [2, 5, 18–20]. Tang et al. [21] investigated the dynamic interaction that occurs between silty-clay soil and an irregular-section subway station. The findings indicated that the motion of the subway station was mostly affected by the characteristics of the adjacent silty-clay soil, specifically in relation to its phase and amplitude. The phenomenon of seismic settlement had a strong correlation with Arias intensity, resulting in non-uniform settlement patterns and the separation of soil and structures. The subway station experienced deformation in a shear mode, necessitating the implementation of stronger structural elements and the use of meticulous seismic design guidelines.

Xin et al. [22] proposed a casing-shape tunnel lining system with internal, exterior, and buffer layers to alleviate constraint effects. The external lining and buffer layer minimize earthquake-induced internal forces, according to Timoshenko composite beam theory. Shaking table experiments confirm the model, showing that fault angle affects lining length, fault slippage directly shears the external lining, and the higher exterior and interior linings are adequately protected. To apply casing-shape tunnel lining in seismic scenarios, the work gives theoretical and experimental insights. The previous studies have not shown any experimental or numerical investigations of the tunnels in Yemen (Sana'a). Also, because of urbanization and housing growth, a tunnel transit system has become necessary. Especially when we consider that all of Yemen's neighbors, including Saudi Arabia, the United Arab Emirates, and Oman, have begun to use tunnels in considerable numbers.

Thus, in the present research work, an experimental soil exploration study has been conducted on the four locations in Sana'a city, Yemen, and the suitability of the chosen sites was assessed for the construction of an underground concrete tunnel system. The geotechnical parameters for tunnel design were evaluated using the finite element package ABAQUS, and two-dimensional plane-strain numerical models of underground tunnel structure were developed to conduct the parametric study in different soil types and boundary conditions under static loading. The material behavior of soil strata has been incorporated into the well-known Mohr-Coulomb constitutive model. At last, the suitability and structural performance of the RC tunnel system were compared at all four sites.

2. Experimental Study

The soil exploration of the four sites was conducted by performing various field and laboratory tests. The wash/rotary boring technique was used to drill holes to the necessary depth. Regular UDS and SPT tests were carried out, and soil samples were correctly identified and labeled when they were brought to the lab. The Standard Penetration Test was performed with a standard split spoon sampler. Once the sampler was fully inserted, it was carefully removed. Both the head and the cutting shoe were taken off. After being correctly labeled with the depth of the bore hole mark, reference number, and other details, the soil samples were sealed in polythene bags and used for visual examination and identification in the process of logging the bore holes. The summarized data sheet has the field "N" values that were recorded at different depths (see Tables 1 to 4). The sub-soil report contained distinct presentations of the test data and boring logs for the soil samples. Soil samples that had not been disturbed were meticulously removed, taking care to preserve the soil's moisture content and structure. Samples of undisturbed soil were collected using a standard open-tube sampler. The sampling tube's bore hole number and depth were marked on the tube for accurate identification, and each end was meticulously sealed with wax.

To determine the different mechanical and physical qualities of the soil, laboratory experiments were performed on the soil samples. The Unconfined Compressive Strength, or "q_u" test (ASTM D 2166), and the Unconsolidated, Undrained Triaxial Compressive Strength, or UU Test (ASTM D 2850), are the two most common types of strength testing. In each of these tests, the compressive strength of the soil was determined by applying an axial load to a cylindrical sample of undisturbed soil until failure. The "q_u" test's lack of laterality confinement, which can result in an early failure and lower compressive strength results, was the main distinction between the two tests. The UU test is usually limited to the lateral stress that the in-situ soil sample was exposed to, and it is conducted laterally within a triaxial chamber. The soil boring log documents the compressive strength and the axial strain at failure (ε_f). Recorded was the confining tension associated with UU testing. The Atterberg's Limit tests (ASTM D 4318) were used to assess the soil's consistency, or "Clayeyness." The Liquid Limit (LL), Plastic Limit (PL), and Plasticity Index (PI), which is the difference between the LL and the PL, make up Atterberg's limit. The distribution of the soil sample's individual particle sizes was ascertained using the ASTM D 422 particle size analysis test. For soils with sand and gravel, the test was conducted using mechanical sieves; for soils with clayey and silty textures, a "hydrometer" was used. Additionally, the soil sample's dry density and moisture content were determined using the ASTM D 2216 standard. Tables 1 to 4 contain tabulations of all the soil parameters for the various sites.

Table 1. Physical and mechanical properties at Site 1

Layer No.	**1**	**2**	**3**	**4**	**5**	**6**	**7**
Average Thickness (m)	**0.80**	**9.0**	**0.75**	**5.30**	**0.90**	**4.0**	**3.0**
			Physical properties				
Specific Gravity (Gs)	2.60	2.63	2.51	2.49	2.60	2.70	2.63
Bulk Density (Ɣ) kN/m^3	18.3	18.7	18.4	18.6	17.9	18.7	19.3
Natural Moisture Content (Wc%)	4.50	6.20	8.38	12.27	21.60	7.00	6.97
Dry Density (Ɣd) kN/m^3	17.5	17.61	16.98	16.57	14.72	17.50	18.04
Natural Void Ratio (e%)	47.9	46.52	45.04	47.44	73.54	53.4	43
Natural Porosity (n%)	32.4	31.75	31.05	32.18	42.38	34.8	30.07
Degree of Saturation (s%)	24.9	35.0	46.7	64.4	76.5	35.7	42.6
Saturated Density (Ɣsat)	20.7	20.7	20	19.7	18.9	20.9	21
Submerged Density (Ɣsub)	10.90	10.90	10.21	9.91	9.07	11.10	11.18
Liquid Limit (LL%)	…….	27.90	27.83	27.90	27.85	27.90	…….
Plastic Limit (PL%)	…….	21.37	23.52	21.37	20.93	21.20	…….
Liquidity Index (LI %)	…….	PL>W	PL>W	PL>W	PL<=Wc<=LL	P.L>Wc	…….
Plastic Index (PI%)	…….	6.53	4.31	6.53	6.92	6.70	…….
Relative Consistency (Cr %)	…….	3.32	4.51	2.39	0.90	3.14	…….
Plasticity	Non plastic	low plastic	Slightly plastic	low plastic	low plastic	low plastic	Non plastic
Consistency	Dense	Dense	Dense	Dense	Medium Stiff	Dense	Dense

Mechanical properties							
Angle of Internal Friction (°)	35.0	36.0	35.0	36.4	26.0	34.7	36.0
Cohesion (C) kN/m^2	0.75	1.2	1.3	3.0	1.3	6.0	0.1
Friction Coeff (σ)	0.53	0.55	0.53	0.56	0.38	0.53	0.55
Standard Penetration (Blwos) (Ncorr)	23	40	36	46	36	40	36
Modulus of Elasticity (Es) kPa	34800	55200	50400	62400	50400	55200	50400
Classification Properties							
Color	Brown	Brown to Gray	Gray Reddish	Brown to Gray	Light Brown	Brown	Light Brown
Gravel (%)	69.40	54.62	16.48	48.15	11.67	49.29	81.35
Sand (%)	29.51	35.30	65.05	30.37	32.81	29.16	17.32
Percentage of Fine Soil (%)	1.04	10.2	18.47	21.09	55.5	21.55	1.33
Classification	(GP) poorly graded gravel with sand	(GP-GM) poorly graded gravel with silt and sand	(SM-SC) silty clayey sand with gravel	(GP-GM) poorly graded gravel with silt and sand	(CL-ML) sandy silt clay	(GM-GC) silty clayey gravel with sand	(GP) poorly graded gravel with sand

Table 2. Physical and mechanical properties at Site 2

Layer No.	**1**	**2**
Average Thickness (m)	**2.0**	**18.0**
Physical Properties		
Specific Gravity (Gs)	2.57	2.61
Bulk Density (Ɣ) kN/m^3	17.5	18
Natural Moisture Content (Wc%)	8.3	5.2
Dry Density (Ɣd KN/m^3)	16.2	17.1
Natural Void Ratio (e%)	55.8	49.6
Natural Porosity (n%)	35.8	33.1
Degree Of Saturation (s%)	37.9	27.2
Saturated Density (Ɣsat)	19.7	20.4
Submerged Density (Ɣsub)	9.9	10.6
Liquid Limit (LL%)	25.7	....
Plastic Limit (PL%)	21	....
Liquidity Index (LI %)	P.L>Wc	....
Plastic Index (PI%)	4.7	....
Relative Consistency (Cr %)	3.68	....
Plasticity	Slightly plastic	Non plastic
Consistency	Very Loose	Dense
Mechanical Properties		
Angle Of Internal Friction (°)	27.2	33.57
Cohesion (C kN/m^2)	9.129	2.448
Friction Coeff (σ)	0.54	0.45
Standard Penetration (Blwos) (Ncorr)	21	43
Modulus of Elasticity (Es kPa)	11520	14700
Classification Properties		
Color	Brown	Yellowish Brown to Gray
Gravel %	35.61	26.80
Sand %	19.23	55.58
Percentage of Fine Soil (%)	45.17	14.22
Classification	(GM- GC) silty clayey gravel with sand	(CL-ML) sandy silt clay with some gravel

Table 3. Physical and mechanical properties at Site 3

Layer No.	**1**	**2**	**3**	**4**	**5**	**6**
Average Thickness (m)	**4.8**	**1.6**	**2.3**	**6**	**2.2**	**5.6**
Physical Properties						
Specific Gravity (Gs)	2.65	2.86	2.74	2.76	2.7	2.66
Bulk Density (Ɣ) kN/m^3	15.6	17.4	16.6	18.3	16.6	17.5
Natural Moisture Content (Wc%)	23.8	18.4	18.9	20.1	17.4	12.1
Dry Density (Ɣd kN/m^3)	12.6	14.7	14	15.2	14.1	15.6
Natural Void Ratio (e%)	16.3	90.9	92.5	77.7	87.3	67.2
Natural Porosity(n%)	51.5	47.6	48	43.7	46.6	40.2
Degree Of Saturation (s%)	59.4	57.8	55.9	71.4	53.8	48
Saturated Density (Ɣsat)	17.7	19.4	18.7	19.5	18.7	19.6
Submerged Density (Ɣsub)	7.8	9.6	8.9	9.7	8.9	9.7
Liquid Limit (LL%)	35.4	35.5	35.3	33.9	33.2	0
Plastic Limit (PL%)	27	28.7	26.2	27.2	26.5	0
Liquidity Index (LI %)	P.L>Wc	P.L>Wc	P.L>Wc	P.L>Wc	P.L>Wc	....
Plastic Index (P.I%)	8.4	6.8	9.2	6.7	6.7	0
Relative Consistency (Cr %)	1.38	2.51	1.8	2.06	2.35	....
Plasticity	low plastic	low plastic	low plastic	low plastic	low plastic	Non plastic
Consistency	Stiff	Dense	Stiff	Dense	Stiff	Dense
Mechanical Properties						
Angle Of Internal Friction (°)	23.5	34.0	30.0	34.0	28.0	34.0
Cohesion (C kN/m^2)	16.6	2.7	7.0	2.7	5.6	2.0
Friction Coeff (σ)	0.34	0.51	0.44	0.51	0.41	0.51
Standard Penetration (Blwos) (Ncorr)	32	46	36	44	31	35
Modulus Of Elasticity (Es) (kPa)	15040	19520	16320	18880	14720	16000
Classification Properties						
Color	Dark Brown	Brown to Gray	Brown	Gray	Light Brown	Brown to Gray
Gravel %	3.21	23.35	6.16	9.68	15.33	26.11
Sand %	23.87	43.4	25.43	51.41	33.67	41.13
Percentage Of Fine Soil (%)	72.92	33.25	68.41	38.91	51	32.76
Classification	fill, silty clayey sand with gravel	(SM-SC) silty clayey sand with gravel	(CL) inorganic clay and very fine sands gravel	(SM-SC) silty clayey sand with gravel	(CL) inorganic clay and very fine sands grave	(SM-SC) silty clayey sand with gravel

Table 4. Physical and mechanical properties at Site 4

Layer No.	**1**	**2**	**3**	**4**	**5**	**6**	**7**
Average Thickness (m)	**1.6**	**1.7**	**2.7**	**4.5**	**2.5**	**3.5**	**5.5**
Physical Properties							
Specific Gravity (Gs)	2.60	2.68	2.66	2.66	2.68	2.65	2.69
Bulk Density (Ɣ) kN/m^3	17.7	18.0	17.2	18.0	18.2	18.4	18.9
Natural Moisture Content (wc%)	13.4	18.5	16.4	18.3	10.8	14.9	7.1
Dry Density (Ɣd kN/m^2)	17.68	17.97	17.17	17.97	18.18	18.37	18.89
Natural Void Ratio (e%)	44.1	46.4	51.9	45.2	44.7	41.8	39.8
Natural Porosity(n%)	43.9	46.2	51.6	45,0	44.5	41.6	39.6
Degree Of Saturation (s%)	79.0	96.0	84.0	97.0	65.0	94.3	48.0
Saturated Density (Ɣsat)	25.4	26.2	26.0	26.0	26.2	26.0	26.3
Submerged Density (Ɣsub)	15.6	16.4	16.2	16.2	16.4	16.2	16.5
Liquid Limit(LL%)	....	....	....	26.18	....	....	....
Plastic Limit(PL%)	....	....	....	19.52	....	....	....
Liquidity Index(LI %)	....	....	....	PL >Wc	....	....	....
Plastic Index (PI%)	....	....	....	6.6	....	....	....
Relative Consistency (Cr %)	....	....	....	1.18	....	....	....
Plasticity	Non plastic	Non plastic	Non plastic	Low plastic	Non plastic	Non plastic	Non plastic

Mechanical Properties							
Angle Of Internal Friction (°)	29	35	27	31	33	34	33
Cohesion (C kN/m^2)	2.039	0.102	7.648	2.039	1.733	0.102	0.714
Friction Coeff (σ)	0.554	0.692	0.501	0.6	0.656	0.671	0.656
Modulus Of Elasticity (Es kPa)	32100	44900	33600	37100	42600	39600	39000
Standard Penetration (Blwos) (Ncorr)	21	41	23	28	37	32	31
Classification Properties							
Color	Yellowish Brown	Brown	Redish Brown	Brown	Light Brown	Brown	Gray
Gravel %	0	5.11	11.99	21.65	55.15	32.14	20.5
Sand %	41.44	11.61	32	52.46	37.05	43.43	67.59
Percentage of Fine Soil (%)	58.56	83.28	56.01	25.89	7.8	24.43	11.91
Classification	(ML) sandy silt	(GW) well graded gravel	(ML) sandy silt	(SC) clayey sand with gravel	(GW-GM) well graded gravel with sand	(SM) silty sand with gravel	(SP -SM) poorly graded sand with silt and gravel

3. Numerical Modeling

In order to investigate the structural performance of the underground tunnel under a variety of soil and boundary conditions, a two-dimensional numerical model of the tunnel was developed in the ABAQUS/CAE module. Following a thorough examination of the relevant literature, a soil domain with dimensions of 45×30 m was selected with the objective of minimizing the impact of the boundaries and simulating the conditions found in the real field [2, 11, 19, 23, 24]. In this study, an RC circular tunnel of 5 m overall diameter and 200 mm thick concrete liner of M30 grade was driven by mechanized tunneling (see Table 5). An overburden soil stratum of 15 m was assumed from the crown of the tunnel. The soil domain was modeled with Mohr-Coulomb's constitutive model with a non-associative flow rule, and the liner was discretized using the elasticity model. In this study, shield tunneling has been simulated by taking into consideration the appropriate stiffness of liner material at various points, as indicated in Tables 1 to 4. Reduced integration, hourglass control, and a bilinear plain strain quadrilateral element with four nodes (CPE4R) have been used to discretize the soil domain and the liner material. Several mesh sensitivity studies were run, and the optimum mesh size was finalized (Figure 1). The soil domain of the mesh consists of 27960 equally spaced quad-type elements (Figure 2). The initial stresses in the soil ahead of excavation were calculated in the geostatic step module given in ABAQUS/Standard. By deactivating the soil components in the excavation area and activating the liner elements, the stiffness reduction method has been used to simulate excavation. To ensure deformation compatibility between the liner and the ground, it is necessary for the nodes of the ground's elements to be in contact via the general surface-to-surface contact algorithm. The stratification effect was simulated by incorporating various soil layers with their respective soil properties.

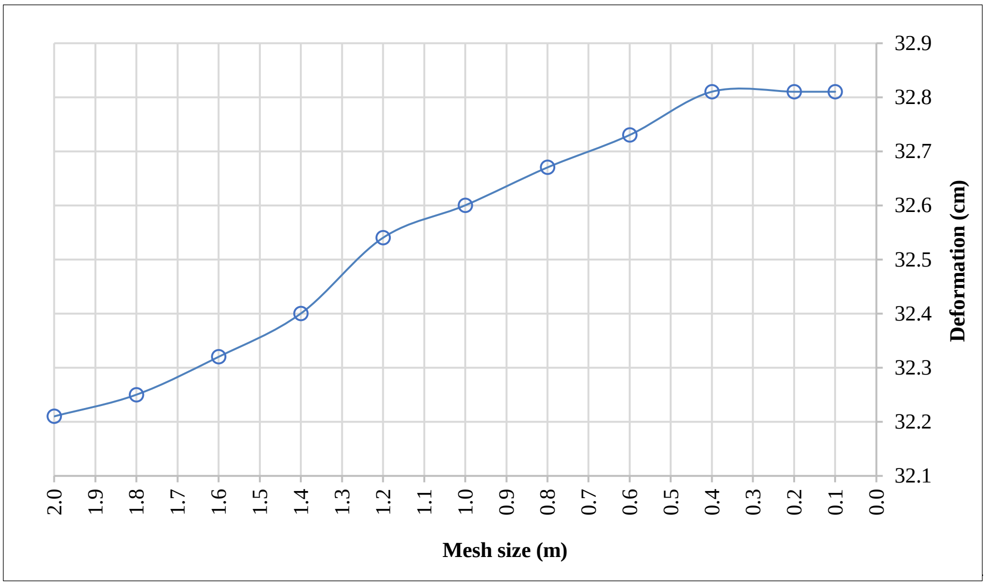

Figure 1. Mesh convergence study for optimum element size of soil domain

Table 5. Input properties of M30 grade concrete

Parameter	Value
Mass density (kg/m^3)	2500
Modulus of elasticity (GPa)	26.6
Poisson's ratio	0.2

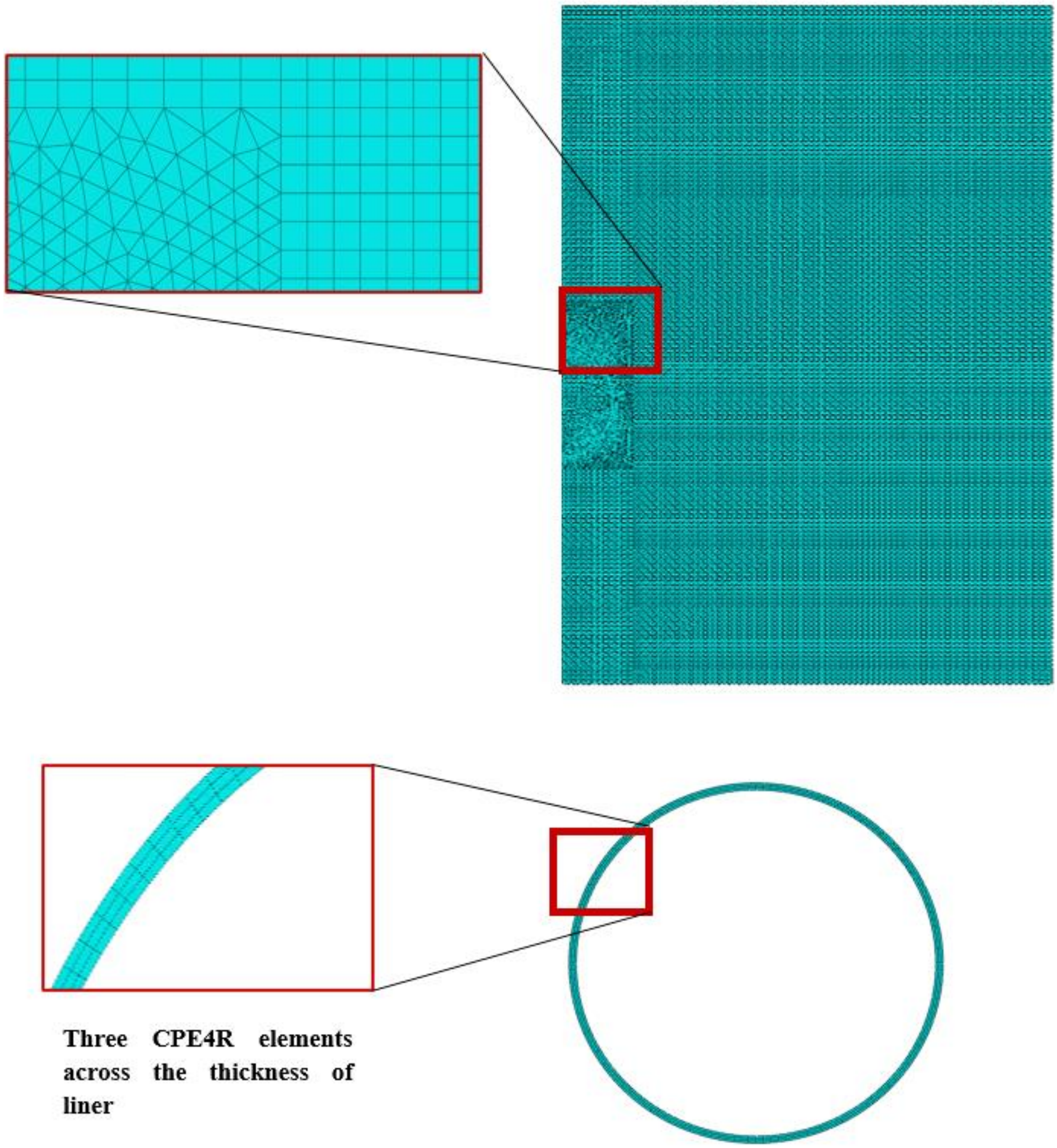

Figure 2. Mesh details of soil domain and RC concrete liner

4. Discussion of Results

After analyzing the soil samples from all four sites, the physical and mechanical properties were extracted and used in the finite element analysis of the soil and tunnel model in the ABAQUS/Standard solver. The numerical study was carried out in order to observe the effect of the stratification of the soil in the area around the opening. The observations were made on the underground RC tunnel structure and soil domain in terms of displacement and stresses. In general, the experimental program and methodology of the current study are presented in the following flowchart for proper tracking of the project process.

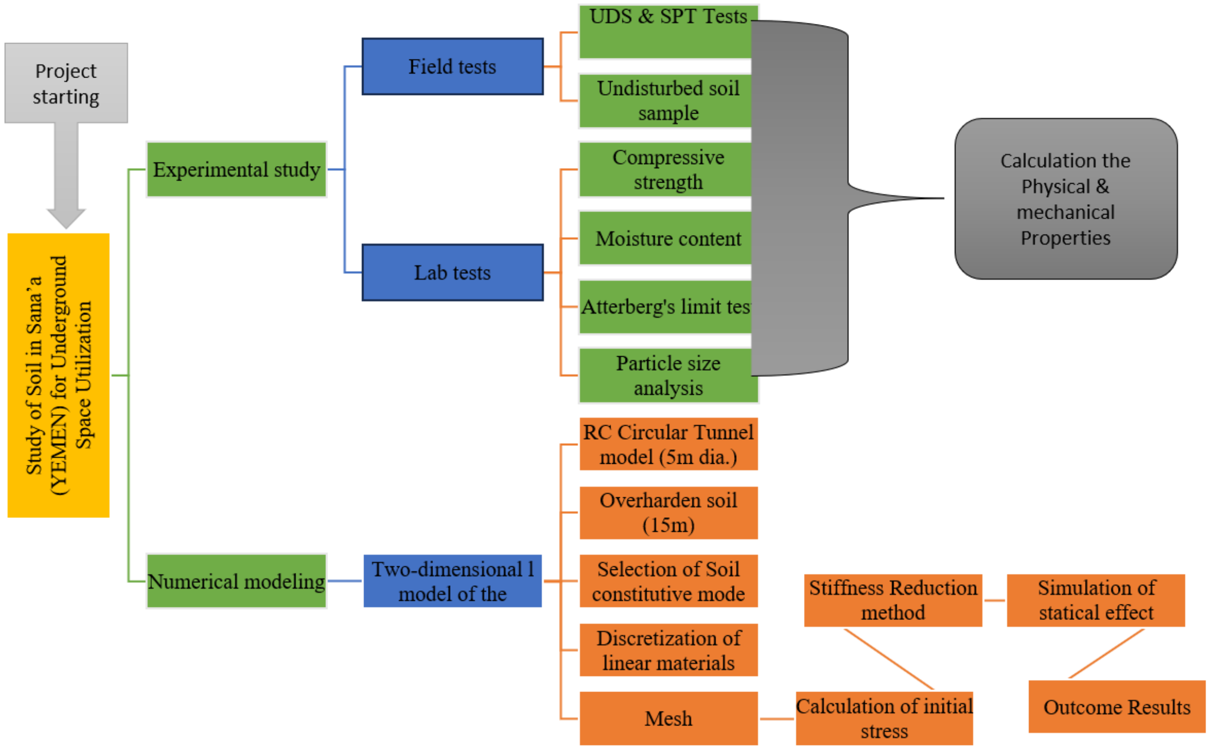

Figure 3. Flowchart of workflow

4.1. Observations at Site

The displacement patterns in the soil domain prior to and after the soil excavation are given in Figure 4. The maximum downward displacement of 136 mm was observed at the topmost layer of the soil. The displacement value increases by 14 cm after excavation and the placement of an RC liner made of concrete. The vertical displacement was found to be reduced as the depth was increased from the top surface to the crown of the tunnel, as observed at Section 1-1, as shown in Figure 5.

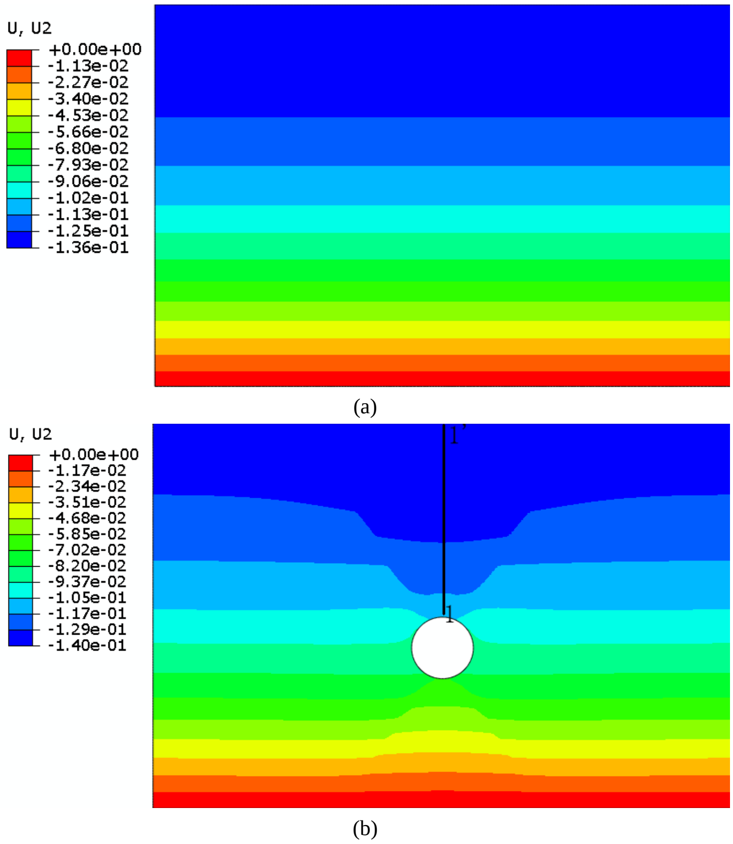

Figure 4. Displacement of soil in (m) at Site 1; (a) before excavation and (b) after excavation

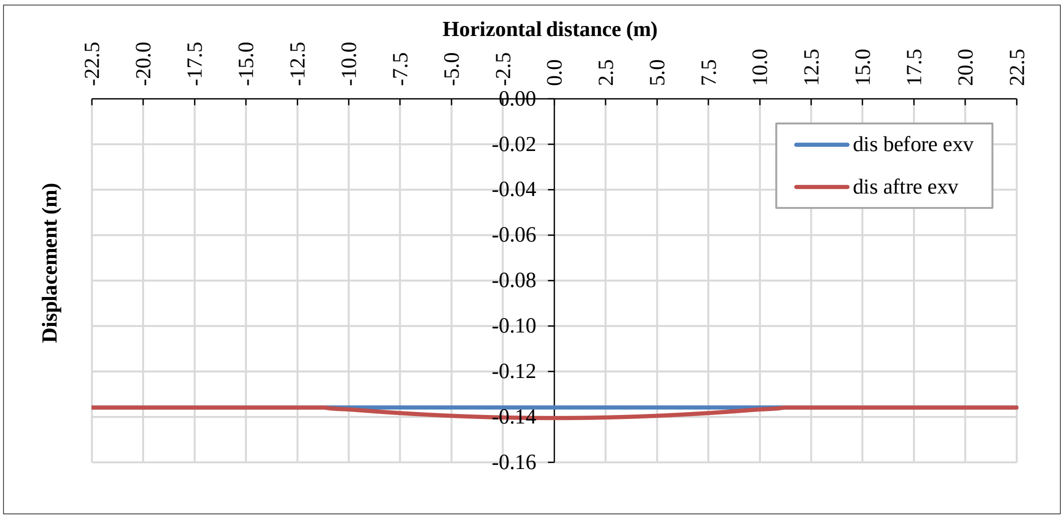

(a)

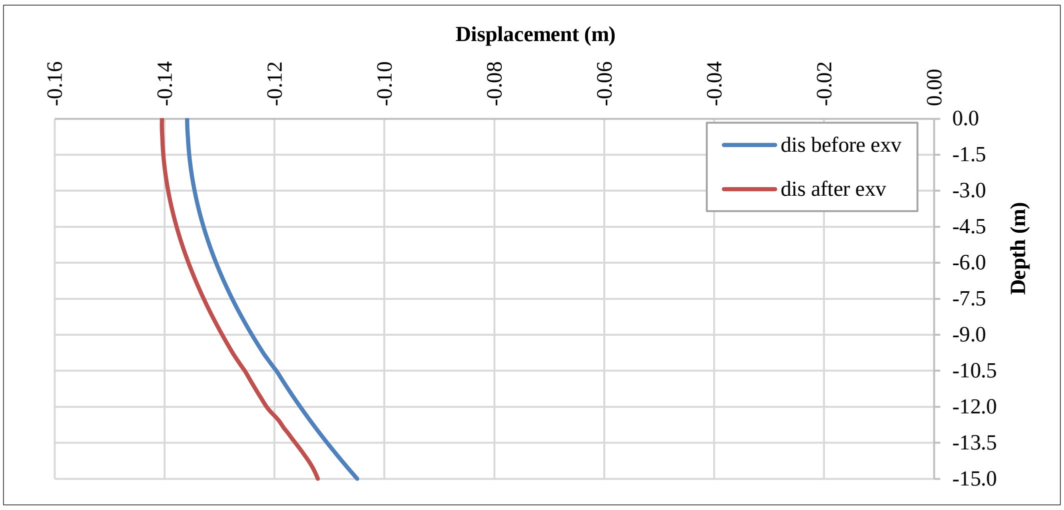

(b)

Figure 5. Displacement in soil in (m) at Site 1 before excavation and after excavation; (a) at top surface and (b) along depth at section 1-1

Figure 6 shows the deformation of the RC liner of the tunnel. The largest amount of displacement (112 mm) occurred at the crown, which was the critical point, and the smallest amount of displacement occurred at the invert, where it measured 67.9 mm. The values for outward displacement at the right springer and the lift springer were both 92.1 mm on both sides.

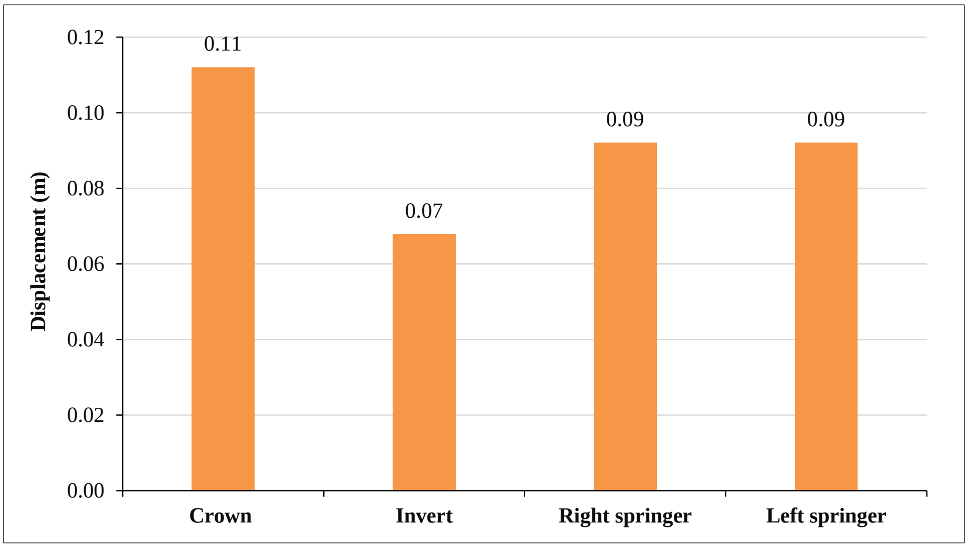

(a)

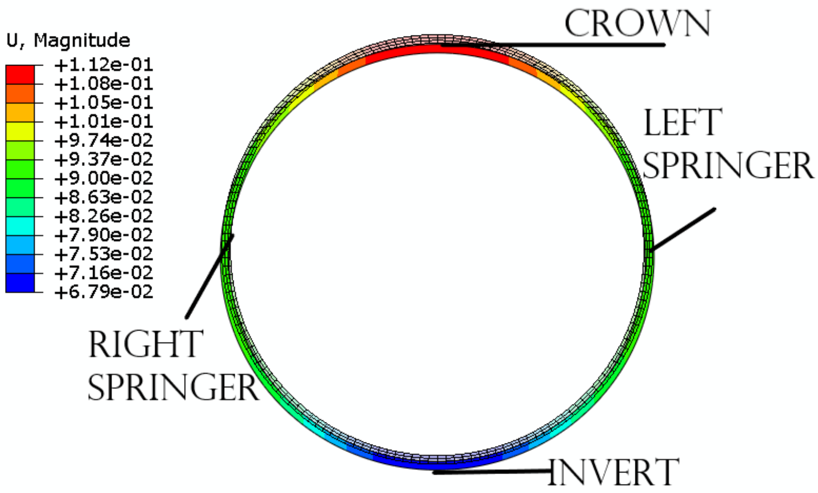

(b)

Figure 6. Deformation in RC liner at Site 1

Tresca stress distribution in the soil before and after excavation has been presented for gravity loads in Figure 7. It could be observed that the excavation process has increased the stress value from 396 kPa to 401 kPa at the base of the tunnel. The stress pattern in the tunnel liner has been presented in Figure 8, and the maximum Maises stress value of 16.2 MPa was observed at the invert.

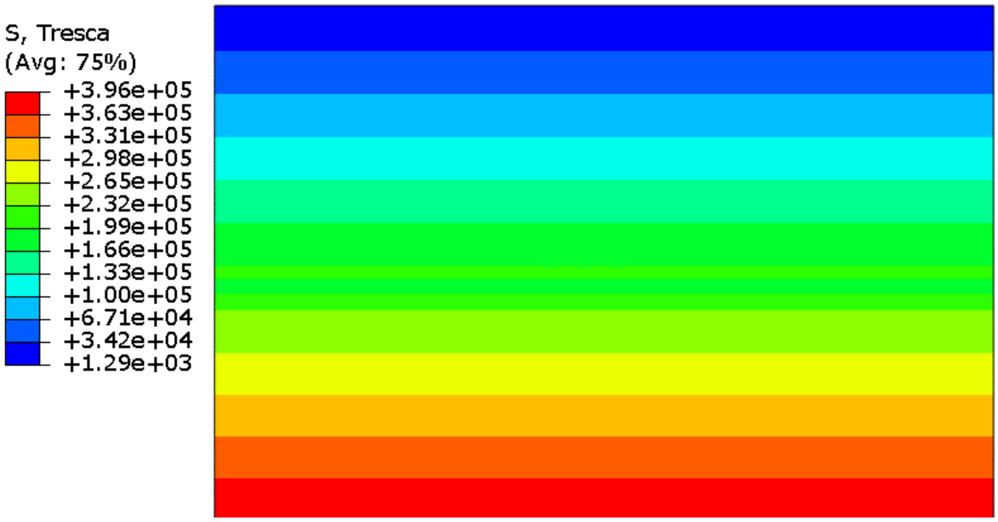

(a)

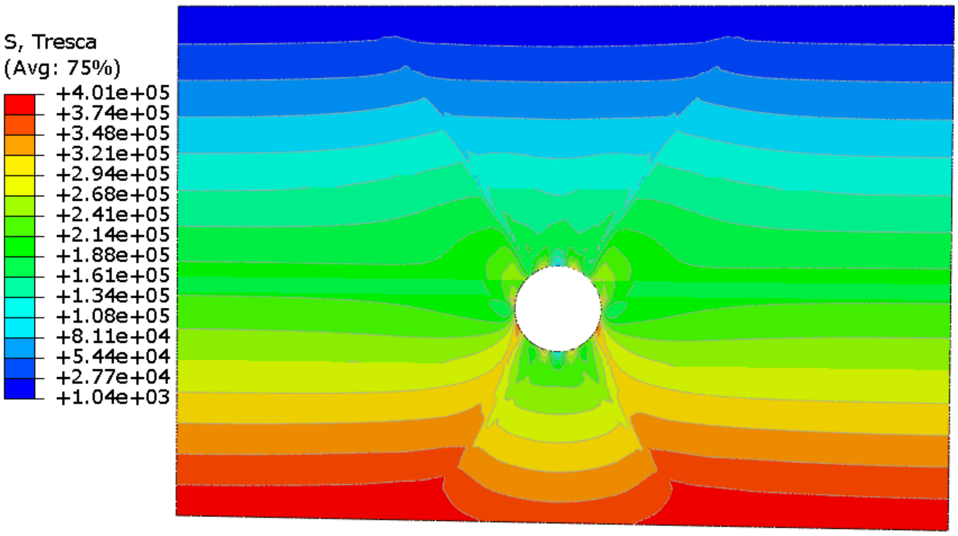

(b)

Figure 7. Tresca stress distribution in the soil; (a) before and (b) after excavation at Site 1

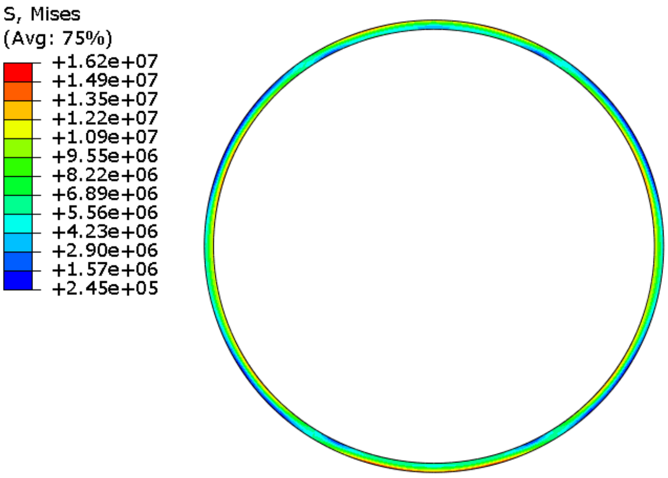

Figure 8. Mises stress distribution in the tunnel liner at Site 1

4.2. Observations at Site 2

There were two layers of soil strata present at Site 2. The displacement pattern of soil strata subjected to gravity has been described in Figure 9. It could be observed that the process of excavation and placement of the tunnel liner has enhanced the soil displacement from 467 mm to 496 mm, exhibiting a 3.52% increase (Figure 10). Further, the vertical displacement was observed to be reduced with an increase in depth.

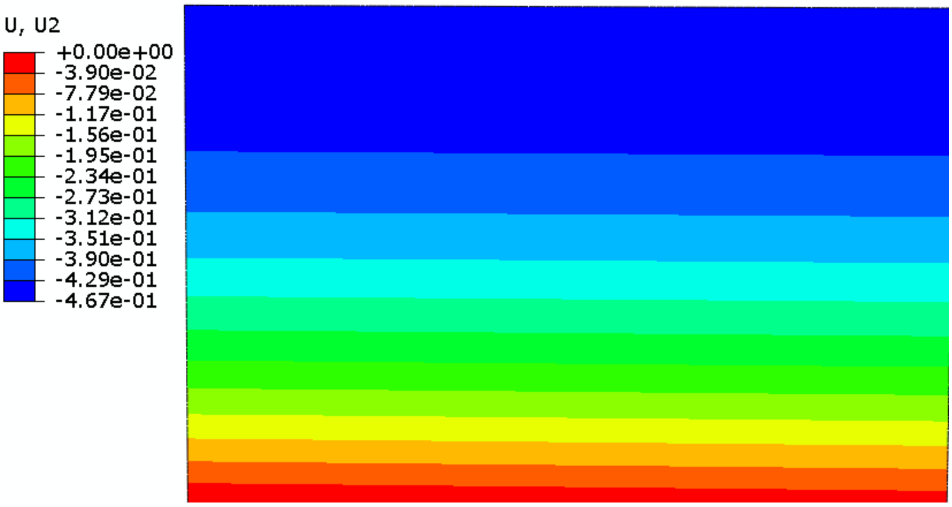

(a)

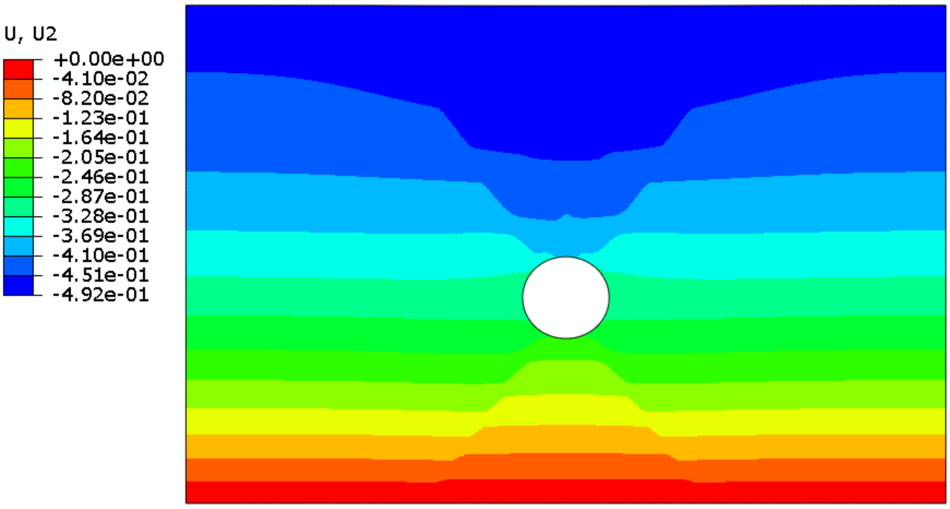

(b)

Figure 9. Displacement of soil in (m) at Site 2; (a) before excavation and (b) after excavation

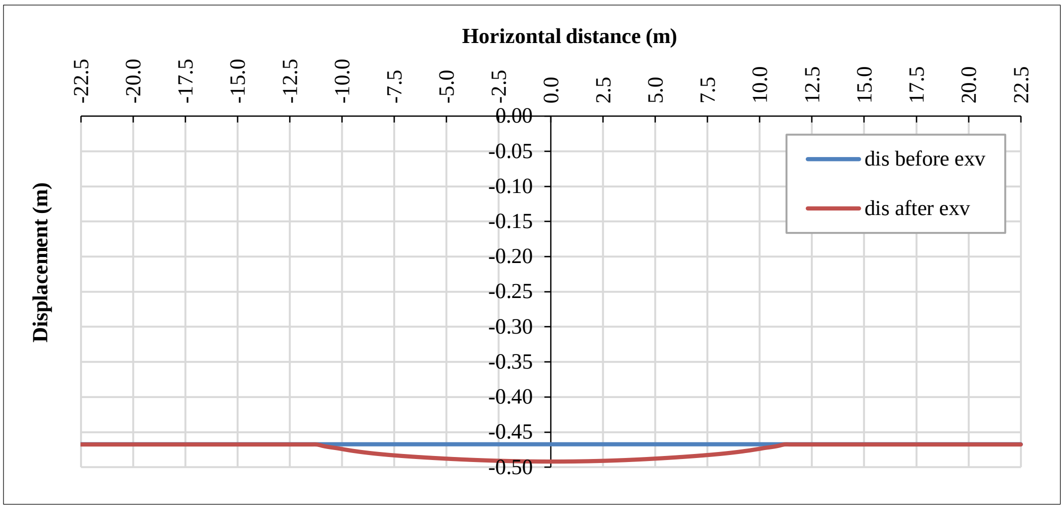

(a)

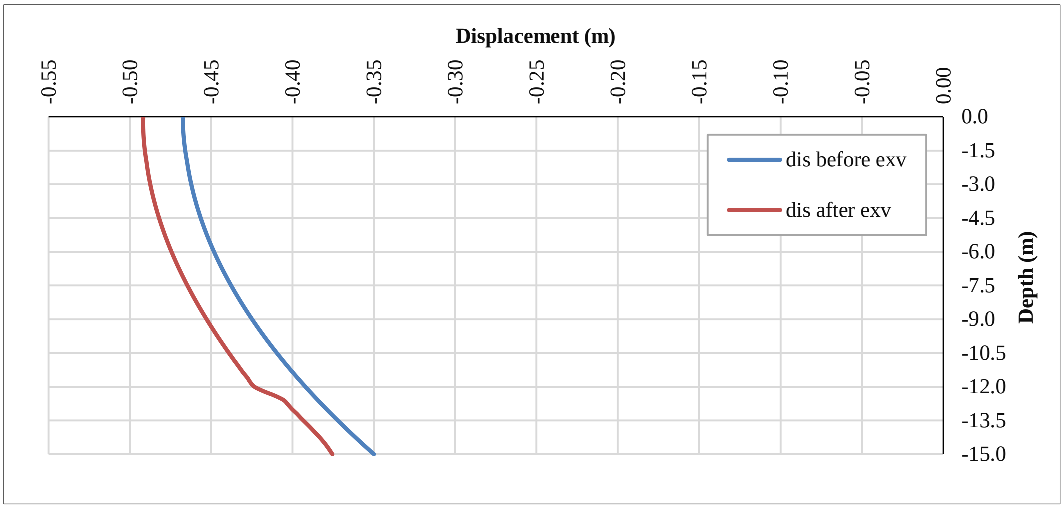

(b)

Figure 10. Displacement in soil in (m) at Site 2 before excavation and after excavation; (a) at top surface and (b) along depth at section 1-1

The overall displacement in the concrete tunnel liner at various locations has been described in Figure 11. A significant amount of displacement of 376 mm was observed at the crown, which is the key point. Whereas, the least significant amount of displacement of 225 mm was found at invert. Both at the right and left springers, the displacement values were found to be equal to 309 mm on both sides.

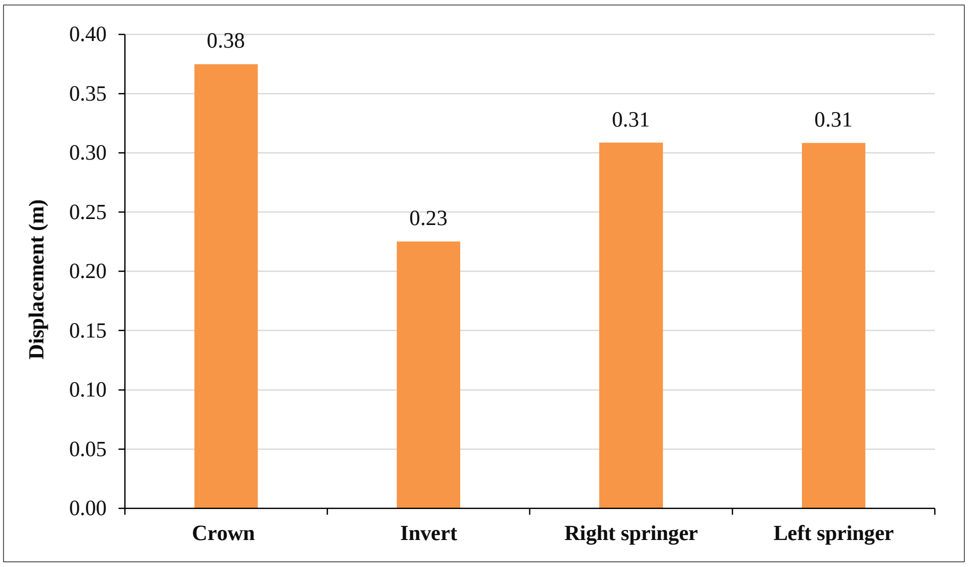

(a)

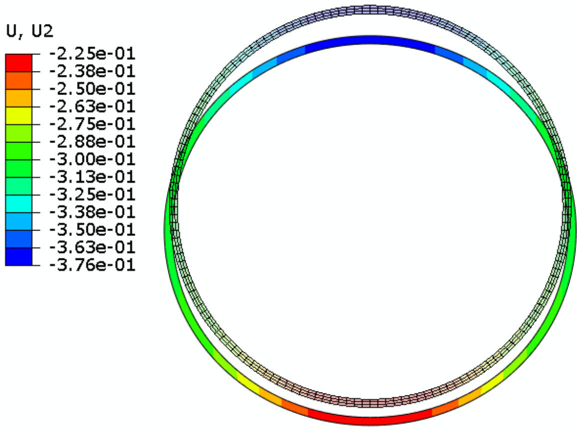

(b)

Figure 11. Deformation in RC liner at Site 2

Figure 12 depicts the characteristics of the Tresca stresses in existing soil strata before excavation. According to the numerical findings, the maximum stress at base of the strata was observed at 378 kPa; however, this value was observed to be increased after excavation and the placement of the concrete liner, reaching a maximum value of 398 kPa, as shown in Figure 12-b. The ratio of the percentage of rise to that of displacement is probably close to 5%

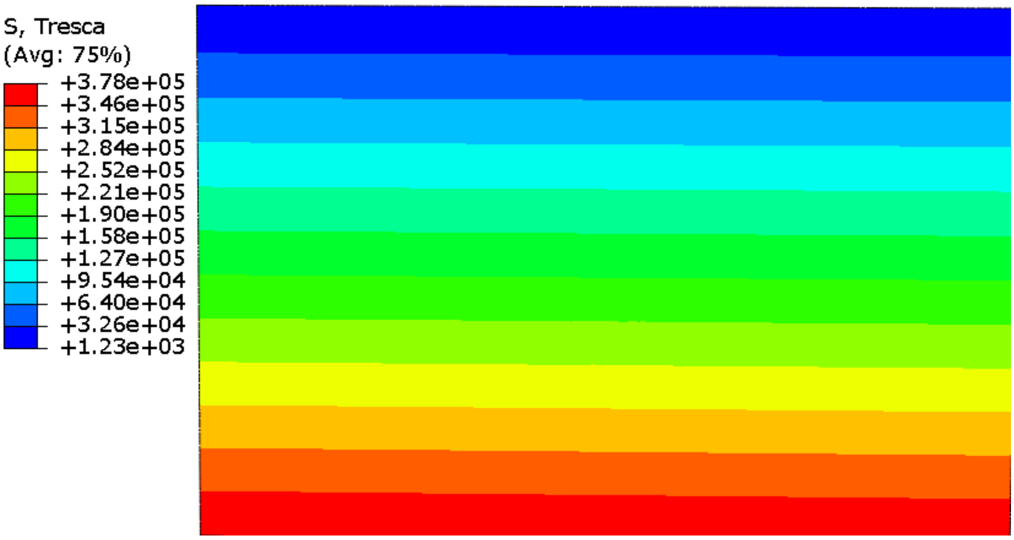

(a)

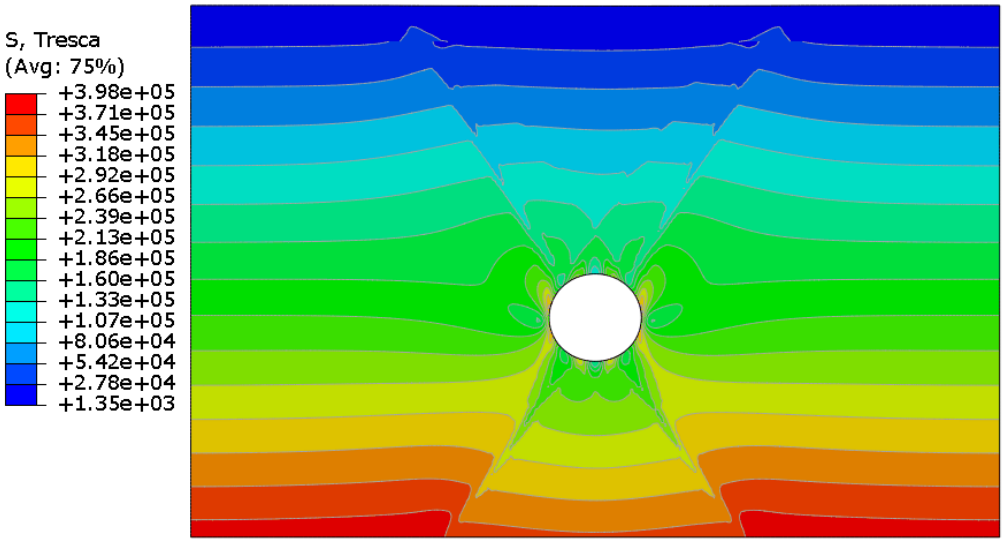

(b)

Figure 12. Tresca stress distribution in the soil; (a) before and (b) after excavation at Site 2

4.3. Observations at Site 3

Site 3 was found to have six different strata of soil. The modeling of a tunnel with a circular shape was carried out at a fixed depth of 15 m below the surface using the data that was obtained from Table 3 in order to evaluate and discuss the various parameters, such as displacement and stress. Figure 13-a illustrates the nature of the displacement of the soil in the vertical part prior to the excavation. According to the results, the highest amount of surface movement that occurs prior to excavation takes place at the very uppermost layer of the surface, where the maximum value is 401 mm. The value of displacement, on the other hand, increased following the excavation and the placement of a lining made of concrete. As shown in Figure 13-b, the maximum amount of displacement takes place at the surface's topmost level and equals 418 mm. As can be seen in Figure 14-a, the percent increase in overall vertical displacement is rather close to being equal to 2.69%. On the other hand, as shown in Figure 14-b, the vertical displacement from the ground surface to the tunnel's crown rises as depth decreases. The ratio of growth to displacement is extremely close to 4.75% in both cases.

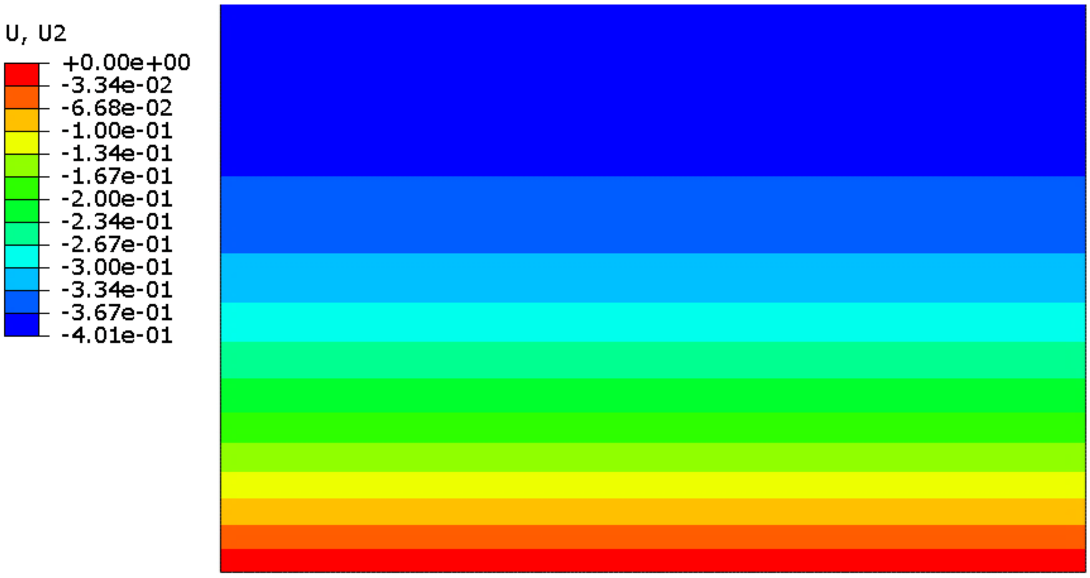

(a)

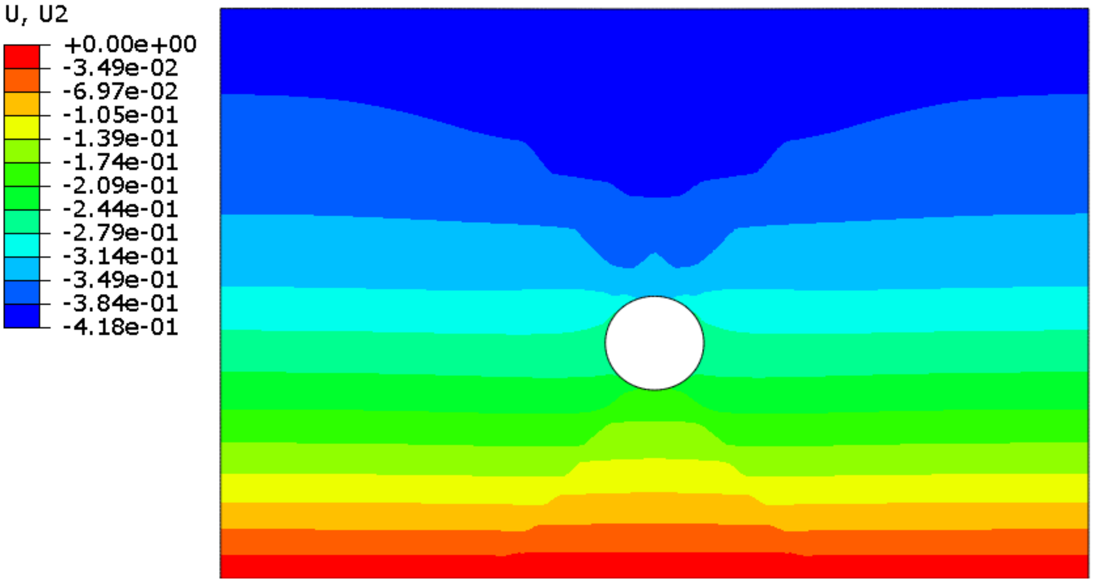

(b)

Figure 13. Displacement of soil in (m) at Site 3; (a) before excavation and (b) after excavation

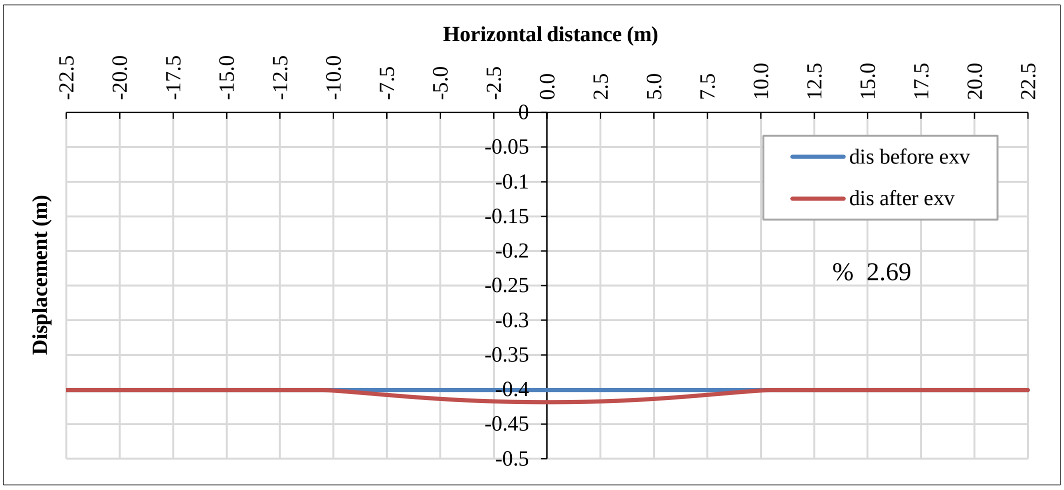

(a)

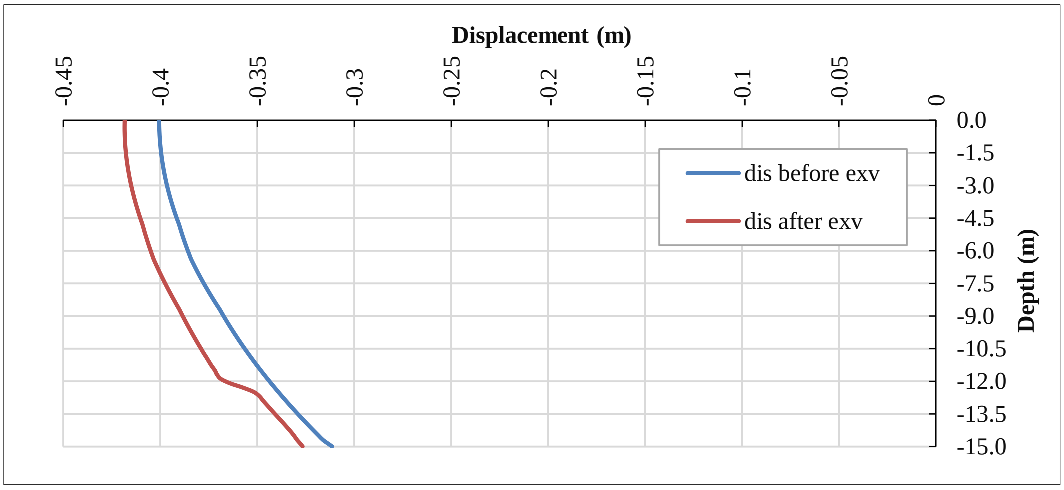

(b)

Figure 14. Displacement in soil in (m) at Site 3 before excavation and after excavation; (a) at top surface and (b) along depth at section 1-1

The displacement of the tunnel's concrete lining has been depicted in Figure 15. The highest value of displacement was observed at the crown at 327 mm, while the invert experienced the least amount of displacement, which measured 197 mm. The displacement values at the left springer and the right springer were both equal to 268 mm.

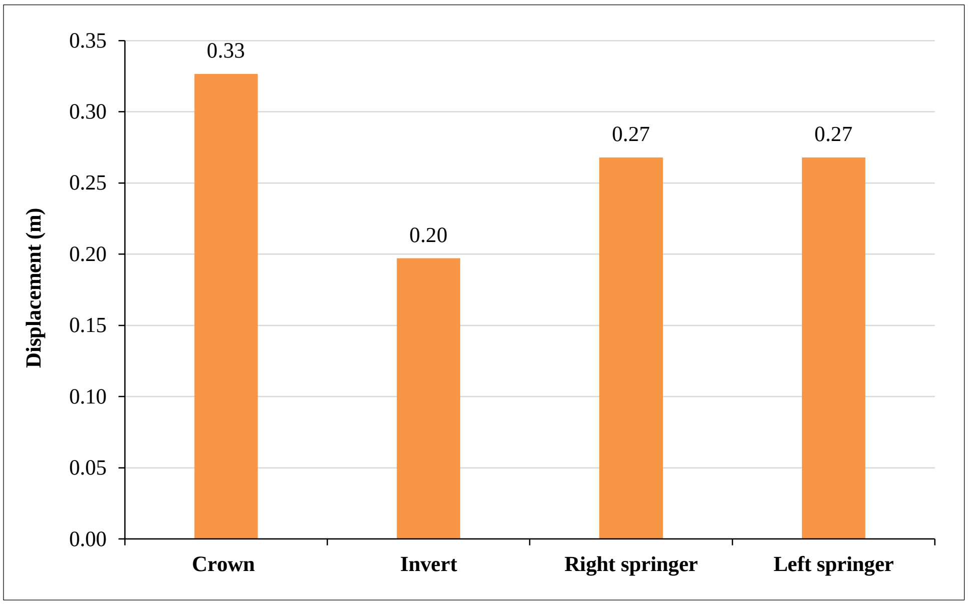

(a)

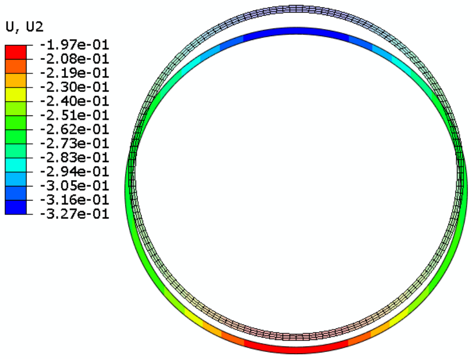

(b)

Figure 15. Deformation in RC liner at Site 3

Figure 16-a illustrates the pattern of the Tresca stress values that existed in the ground prior to excavation. The greatest stress that could have been measured, per the findings, was 363 kPa; nevertheless, this value increased upon excavation and the placement of the concrete liner, reaching a maximum of 378 kPa, as shown in Figure 16-b. The percentage rise to that of displacement is most likely close to 3.96%.

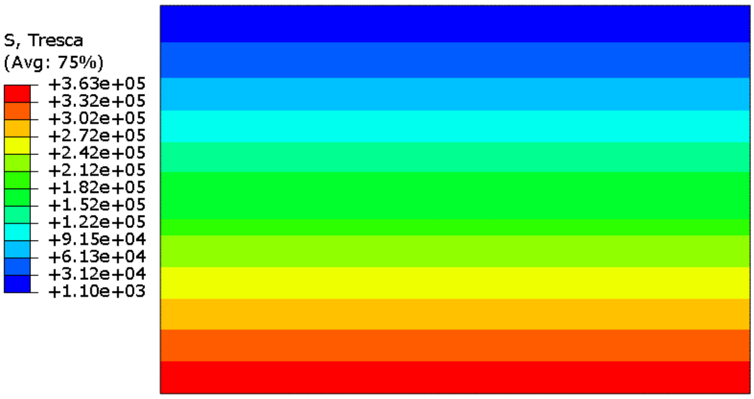

(a)

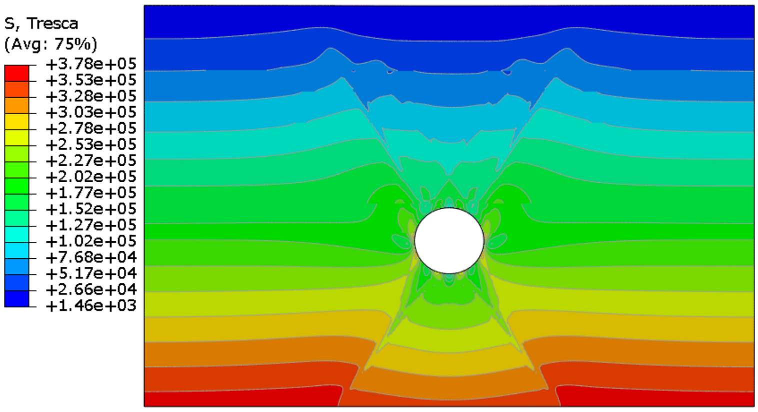

(b)

Figure 16. Tresca stress distribution in the soil; (a) before and (b) after excavation at Site 3

4.4. Observations at Site 4

The strata at Site 4 were found to be made up of seven separate soil layers. Using the data from Table 4, a circular tunnel was modeled at a fixed depth of 15 m below the surface in order to assess and examine the various characteristics, such as displacement and stress. The pattern of soil displacement in the vertical area before the excavation is shown in Figure 17-a. The findings show that the topmost layer of the surface, where the maximum value is 181mm, experiences the greatest degree of surface movement prior to excavation. On the other hand, after excavation and the installation of a concrete lining, the value of displacement rises. The largest displacement, which is 192 mm, occurs at the uppermost level of the surface, as depicted in Figure 17-b. Figure 18-a shows that the proportion of increase displacement is very nearly equivalent to 3.2%. Contrarily, as illustrated in Figure 18-b, the vertical displacement between the tunnel's top surface and its crown always increases as the depth lowers. In both instances, the growth-to-displacement ratio is quite close to 3.72%.

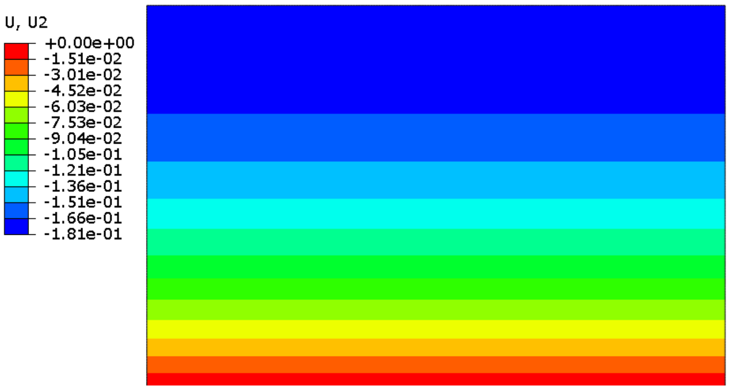

(a)

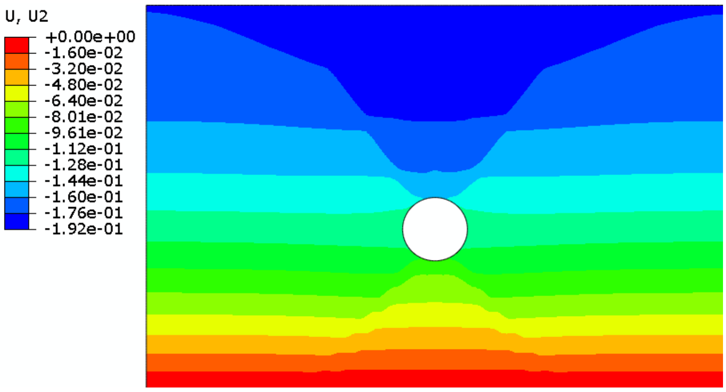

(b)

Figure 17. Displacement of soil in (m) at Site 4; (a) before excavation and (b) after excavation

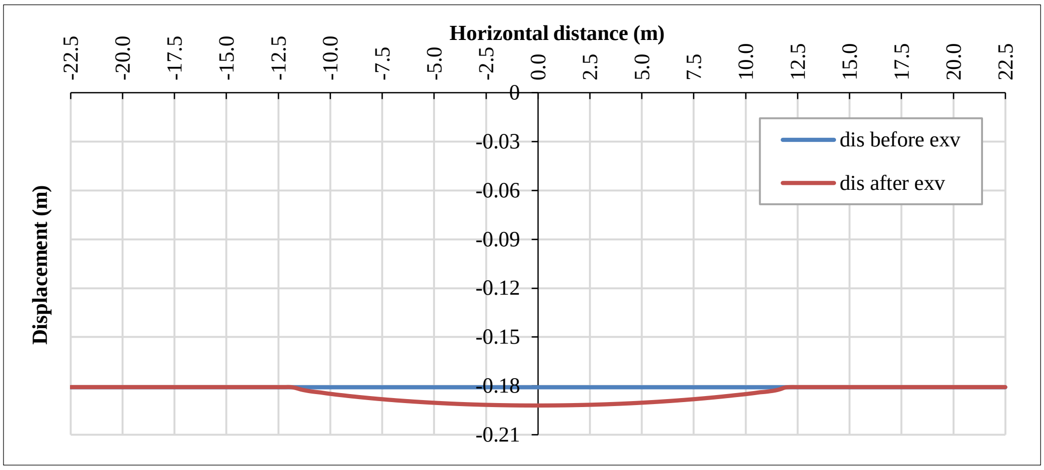

(a)

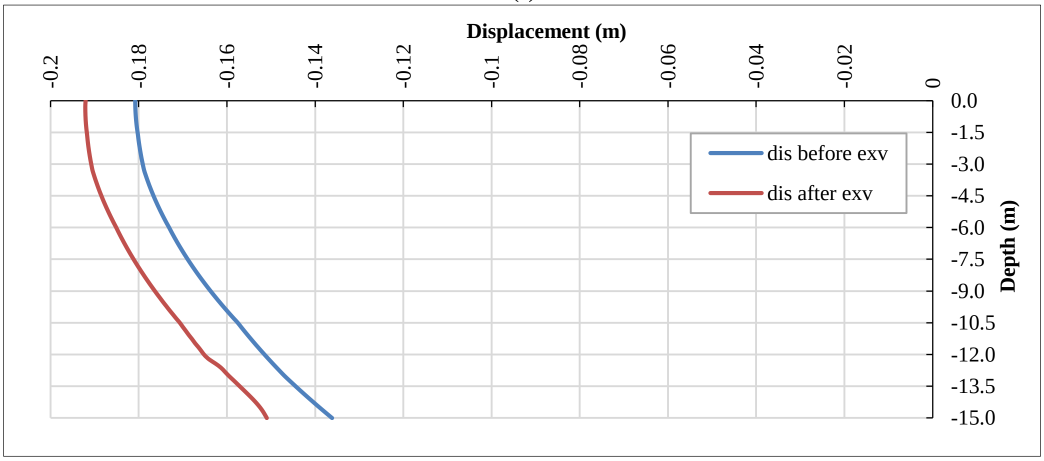

(b)

Figure 18. Displacement in soil in (m) at Site 3 before excavation and after excavation; (a) at top surface and (b) along depth at section 1-1

Figure 19 illustrates the movement of the concrete lining that surrounds the tunnel. At the crown of the concrete liner, the highest amount of movement was observed, which was measured to be 151 mm, while the invert experienced the least amount of movement, which was measured as 85.6 mm. The left springer and the right springer showed the same amount of displacement, which was equivalent to 122 mm.

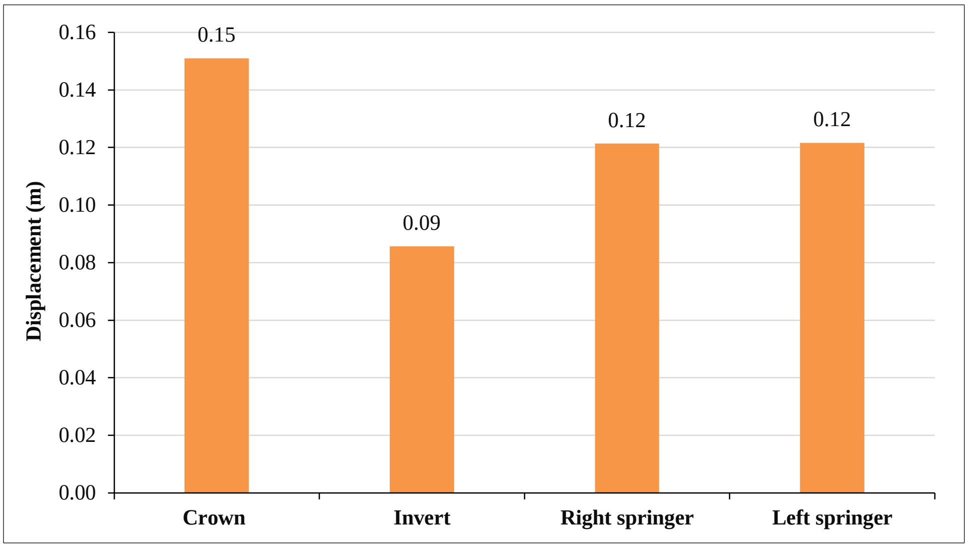

(a)

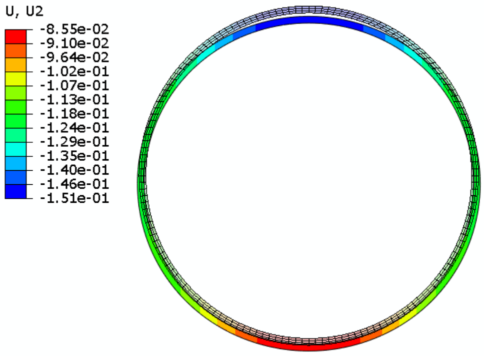

(b)

Figure 19. Deformation in RC liner at Site 4

Figure 20-a depicts the characteristics of the Tresca stress that were present in the ground before the excavation took place. According to the data, the highest amount of stress that could have been observed was 381 kPa; nevertheless, this value was increased during excavation and the placement of the concrete liner, reaching a maximum of 401 kPa, as shown in Figure 20-b. It is highly likely that the ratio of rise to displacement is somewhere around 4.98%. According to Figure 20-b, the tunnel's Mises stress after excavation was found to be 20.7 MPa.

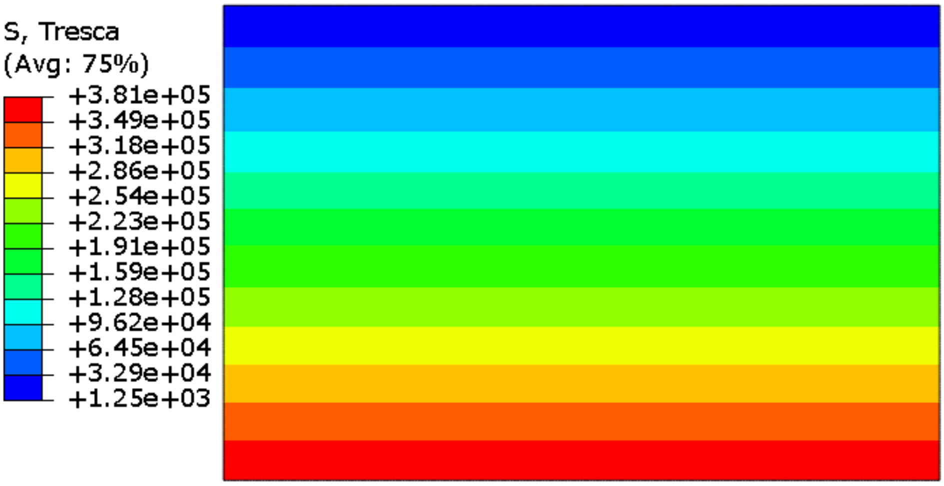

(a)

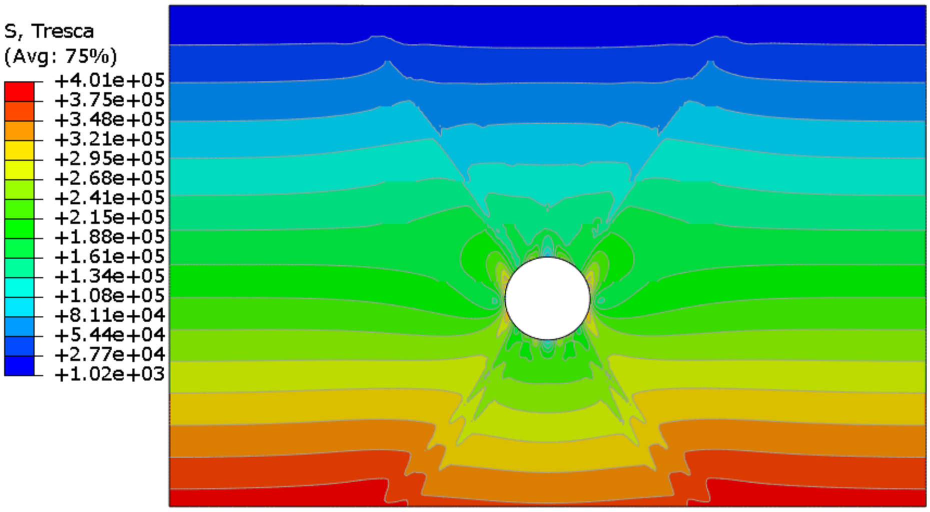

(b)

Figure 20. Tresca stress distribution in the soil; (a) before and (b) after excavation at Site 4

5. Conclusions

In the current capital of Yemen, Sana'a, a time-efficient and economical transportation system is one of the greatest challenges to overcome the increasing urbanization for many years. For rapid transport systems, tunnel structures play a pivotal role in reaching the most unapproachable locations within the city. This present research work has presented experimental soil exploration in Sana'a, Yemen, for searching out the possible locations for tunneling to develop a rapid transportation system in Sana'a city. The field exploration, in-situ, and laboratory soil testing were performed at the four locations with the collaboration of the Ministry of Public Works & Highways, Yemen. Further, to calculate the geotechnical parameters for tunneling, a numerical investigation was carried out using the finite element package ABAQUS software. The geotechnical parameters obtained from the analysis were discussed in terms of effective settlement, deformation in tunnel structure, and the formation of stress patterns in soil and concrete tunnel liner. The following conclusions have been drawn from the presented research work:

- It has been found from the field investigation that the geotechnical properties of the soil strata in Sana'a have a lot of variation.
- From the experimental program, it was observed that sites 1, 2, 3, and 4 were suitable for tunnel structure as they showed less variation in modulus of elasticity, cohesion, and internal angle of friction value between the layers of soil.
- It has been observed that the maximum ground settlement at sites 1, 2, 3, and 4 was approximately 4 mm, 25 mm, 17 mm, and 11 mm, respectively.
- The maximum deformation in the concrete liner of the tunnel was observed at the crown of the tunnel. The ovalling effect was also seen in all the tunnel models.
- The deformation ascertained at the crown of the tunnel was found to be 0.14%D, 0.6%D, 0.302%D, and 0.274%D at sites 1, 2, 3, and 4 respectively, where D is the overall diameter of the tunnel.

6. Declarations

6.1. Author Contributions

Conceptualization, M.R.S., Z.M., and S.H.K.; methodology, M.R.S. and Z.M.; software, O.A., M.R.S., and Z.M.; validation, O.A., M.R.S., and Z.M.; formal analysis, O.A. and M.R.S.; investigation, O.A. and M.R.S.; resources, O.A. and S.H.K.; data curation, O.A.; writing—original draft preparation, O.A.; writing—review and editing, O.A., Z.M., and S.H.K.; visualization, O.A., M.R.S., and Z.M.; supervision, M.R.S. and Z.M.; project administration, M.R.S.; funding acquisition, S.H.K. All authors have read and agreed to the published version of the manuscript.

6.2. Data Availability Statement

The data that support the findings of this study are available on request from the corresponding author.

6.3. Funding

This paper was supported by the United Arab Emirates University (UAEU) under the Research Start-up Proposal with Proposal Number 1967 and Grant Code G00003791. The proposal, which was awarded, was spearheaded by Sanan Husain Khan, affiliated with the College of Engineering-Mechanical & Aerospace Engineering.

6.4. Conflicts of Interest

The authors declare no conflict of interest.

7. References

[1] Khan, M. A., Sadique, M. R., & Alam, M. M. (2017). Stress analysis of tunnel in soft soil: a state of art report. International Journal of Advance Research in Science and Technology, 6(03), 187-195. doi:10.13140/RG.2.2.22765.64482.

[2] Nunes, M. A., & Meguid, M. A. (2009). A study on the effects of overlying soil strata on the stresses developing in a tunnel lining. Tunnelling and Underground Space Technology, 24(6), 716–722. doi:10.1016/j.tust.2009.04.002.

[3] Mazek, S. A., & Almannaei, H. A. (2013). Finite element model of Cairo metro tunnel-Line 3 performance. Ain Shams Engineering Journal, 4(4), 709–716. doi:10.1016/j.asej.2013.04.002.

[4] Chengzhang, J., Cheng, J., & Jiang, Q. (2023). Numerical conformal mapping for underground tunnels with arbitrary shapes based on Symm's method. doi:10.21203/rs.3.rs-3257360/v1.

[5] Zhang, D. ming, Huang, H. wei, Hu, Q. fang, & Jiang, F. (2015). Influence of multi-layered soil formation on shield tunnel lining behavior. Tunnelling and Underground Space Technology, Volume 47. Tunnelling and Underground Space Technology, 47, 123–135. doi:10.1016/j.tust.2014.12.011.

[6] Zhao, G., Wang, D., Shi, L., & Wang, S. (2023). Influences of EDZ and Cross-Section Shapes on Spalling Failure Depth of Non-circular Tunnels in Gneissic Granite. Geotechnical and Geological Engineering, 41(1), 91–105. doi:10.1007/s10706-022-02264-w.

[7] Ali Khan, M., Sadique, M. R., & Zaid, M. (2019). Effect of Stratification on Underground Opening: A Numerical Approach. Lecture Notes in Civil Engineering, 34, 133–142. doi:10.1007/978-981-13-7162-2_11.

[8] Esmaeili, M., Hosseini Manoujan, J., Chalabii, J., Astaraki, F., & Movahedi Rad, M. (2023). Numerical Investigation of the Effect of Longitudinal Fiberglass Dowels on Tunnel Face Support in Layered Soils. Infrastructures, 8(10), 138. doi:10.3390/infrastructures8100138.

[9] Zaid, M., Mishra, S., Rao, K.S. (2020). Finite Element Analysis of Static Loading on Urban Tunnels. Geotechnical Characterization and Modelling. Lecture Notes in Civil Engineering, 85, Springer, Singapore. doi:10.1007/978-981-15-6086-6_64.

[10] Naqvi, M. W., Akhtar, M. F., Zaid, M., & Sadique, M. R. (2021). Effect of Superstructure on the Stability of Underground Tunnels. Transportation Infrastructure Geotechnology, 8(1), 142–161. doi:10.1007/s40515-020-00119-6.

[11] Abbas, H. O. (2020). Influence of Tunnel Excavation on Tower Foundation Settlement Constructed on Sandy Soil. Transportation Infrastructure Geotechnology, 7(4), 651–663. doi:10.1007/s40515-020-00114-x.

[12] Dziuban, B., Ling, H. I., & Li, L. (2018). Failure Mechanisms of Shallow Tunnel in Sandy Ground. Transportation Infrastructure Geotechnology, 5(4), 318–331. doi:10.1007/s40515-018-0062-1.

[13] Kumar, P., & Kumar Shrivastava, A. (2022). Experimental and numerical analysis of deformation behaviour of tunnels under static loading conditions. Sustainable Energy Technologies and Assessments, 52. doi:10.1016/j.seta.2022.102057.

[14] Bian, X., Hong, Z. S., & Ding, J. W. (2016). Evaluating the effect of soil structure on the ground response during shield tunnelling in Shanghai soft clay. Tunnelling and Underground Space Technology, 58, 120–132. doi:10.1016/j.tust.2016.05.003.

[15] Azadi, M. (2011). The seismic behavior of urban tunnels in soft saturated soils. Procedia Engineering, 14, 3069–3075. doi:10.1016/j.proeng.2011.07.386.

[16] Abdel-Motaal, M. A., El-Nahhas, F. M., & Khiry, A. T. (2014). Mutual seismic interaction between tunnels and the surrounding granular soil. HBRC Journal, 10(3), 265–278. doi:10.1016/j.hbrcj.2013.12.006.

[17] Gomes, R. C., Gouveia, F., Torcato, D., & Santos, J. (2015). Seismic response of shallow circular tunnels in two-layered ground. Soil Dynamics and Earthquake Engineering, 75, 37–43. doi:10.1016/j.soildyn.2015.03.012.

[18] Yüksel, Y. Z., & Akbaş, Ş. D. (2023). Static stress analysis of multi-layered soils with twin tunnels by using finite and infinite elements. Geomechanics and Engineering, 33(4), 369–380. doi:10.12989/gae.2023.33.4.369.

[19] Katebi, H., Rezaei, A. H., & Hajialilue-Bonab, M. (2013). The influence of surface buildings and ground stratification on lining loads applying the finite element method. Electronic Journal of Geotechnical Engineering, 18, 1845-1861.

[20] Chai, S., Yan, Y., Hu, B., Wang, H., Hu, J., Chen, J., Fu, X., & Zhou, Y. (2023). The Optimization of Secondary Lining Construction Time for Shield Tunnels Based on Longitudinal Mechanical Properties. Applied Sciences (Switzerland), 13(19), 10772. doi:10.3390/app131910772.

[21] Tang, B., Li, X., Chen, S., Zhuang, H., & Chen, H. P. (2020). Investigations of seismic response to an irregular-section subway station structure located in a soft clay site. Engineering Structures, 217. doi:10.1016/j.engstruct.2020.110799.

[22] Xin, C. L., Wang, Z., Hajirasouliha, I., Yang, F., Li, W. H., Chen, T., & Gao, B. (2022). Seismic response mechanisms of casing-shape composite tunnel lining: Theoretical analysis and shaking table test verification. Soil Dynamics and Earthquake Engineering, 162. doi:10.1016/j.soildyn.2022.107440.

[23] Ahmed, S., Rehan Sadique, M., Ali Khan, M., & Sawant, V. A. (2020). Numerical analysis of behavior of single pile in layered soil against lateral load. Lecture Notes in Civil Engineering, 35, 163–169. doi:10.1007/978-981-13-7480-7_14.

[24] Kiani, M., Akhlaghi, T., & Ghalandarzadeh, A. (2016). Experimental modeling of segmental shallow tunnels in alluvial affected by normal faults. Tunnelling and Underground Space Technology, 51, 108–119. doi:10.1016/j.tust.2015.10.005.